

pubs.acs.org/JPCB Article

Janus Nanoparticle and Surfactant Effects on Oil Drop Migration in Water under Shear

Thao X. D. Nguyen, Sepideh Razavi,* and Dimitrios V. Papavassiliou*



Cite This: J. Phys. Chem. B 2022, 126, 6314-6323



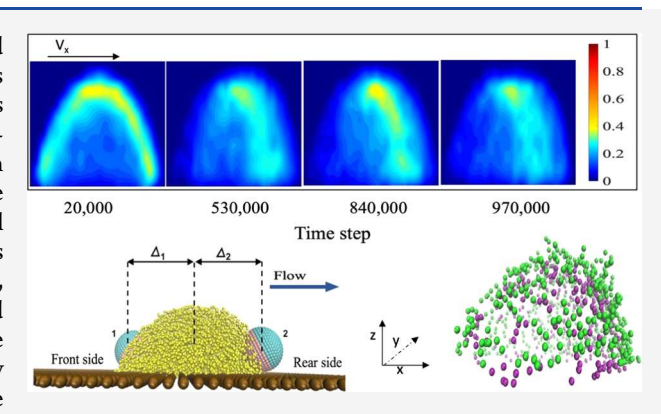
ACCESS I

III Metrics & More

Article Recommendations

Supporting Information

ABSTRACT: The effects of surface-active nanoparticles and surfactants on the behavior of oil—water interfaces have implications for a variety of industrial processes related to multiphase flows including separation processes, enhanced oil recovery, and environmental remediation. In this work, the migration of an oil droplet in shear flow is investigated with the presence of surface-active molecules and nanoparticles at the oil—water interface. Pure oil (heptadecane) in water and oil with the presence of Janus nanoparticles (JPs) and/or octaethylene glycol monododecyl ether, a nonionic surfactant, were examined using coarse-grained computations. The shear flow field was created utilizing a Couette flow, where the top wall of a channel moved with a specified velocity and the bottom wall was kept stationary. The dissipative particle



dynamics (DPD) method was applied. The oil drop was placed on the stationary wall, and its displacement was recorded over time. When surfactants were added at the oil—water interface, the slip of the water over the oil drop was reduced, leading to a larger displacement of the drop. Moreover, surfactant molecules tended to concentrate toward the rear side of the oil drop rather than the front as the drop moved in the flow field. The presence of only JPs on the oil—water interface resulted in slower droplet migration. In the presence of both JPs and surfactants, the effect of JPs on the oil—surfactant—water system was investigated by changing the number of JPs on the drop surface while keeping the concentration of the surfactant constant. Under the same shear rate, the droplet's migration speed increased in the presence of both surfactants and JPs compared to the case of bare oil. The JPs appeared to follow a repeated pattern of motion while residing close to the solid substrate—oil drop contact line. These findings elucidate the contribution of both surfactants and JPs on oil drop displacement for enhanced oil recovery or remediation of an oil-contaminated subsurface.

1. INTRODUCTION

The motion of liquid droplets is important to a broad range of process industries 1-3 and especially the petrochemical sector, where oil and water are often produced and transported together.^{4,5} Several techniques can be exploited to make droplets move, such as electrostatic actuation, ^{16,7} surface energy gradient, ^{8,9} or external forcing by shear flow, ^{10–13} and several studies regarding the transportation of droplets have been performed either experimentally 10,11 or computationally. 13,14 Notably, most previous studies focused on the motion of droplets or bubbles in a cylindrical capillary. 15-17 For noncylindrical geometries, Horwitz et al. studied the effect of the dimensionless parameters (Reynolds number and capillary number) and of the viscosity ratio between the droplet and the carrier fluid on droplet deformation in a square duct.¹⁸ More recently, Luo et al. 13 used a three-dimensional front-tracking finite-difference method to study the effects of the surfactant, including the reduced surface tension and the Marangoni stress, on the motion of a droplet in a square microchannel.

An important aspect that needs examination is the presence of additives or impurities, which may play the role of surfaceactive species. For instance, surfactants are conventionally used for flushing residual oil in hydrocarbon reservoirs through chemical flooding in enhanced oil recovery (EOR) processes. Surfactants can stabilize droplets by reducing the interfacial tension (IFT) at the oil—water interface. In particular, octaethylene glycol monododecyl ether (C12E8) is a common nonionic surfactant used for EOR. In our prior research studies, this surfactant has been employed to explore the effects of surfactants on flat oil—water interfaces in the case of compression of flat interfaces and on the behavior of the multiphase flow. Nanoparticles also affect interfacial behavior, as prior research has demonstrated that nanoparticles can stabilize emulsions, can affect substrate wettability, 26,27

Received: May 27, 2022 Revised: July 30, 2022 Published: August 15, 2022





and can increase the oil recovery rate for EOR.²⁸ Janus nanoparticles (JPs), which are a class of nanoparticles possessing amphiphilicity, are also shown to impact the properties of fluid–fluid interfaces and their response to applied stresses.^{29–36}

The coexistence of surfactants and nanoparticles on the oilwater interface has broad applications in energy and environmental areas. Hence, many studies have focused on the synergies of these surface-active substances.^{37–39} Nourafkan et al. used nanoparticles (TiO₂) as carriers for mixtures of anionic and nonionic surfactants to control the delivery of surfactants to the oil-water interface in EOR applications. 40 As a result, the nanoparticles reduced the surfactant adsorption on a sandstone rock surface, leading to increased oil recovery compared to chemical flooding with surfactants alone. Vu et al. 41 discussed the impact of nanoparticle surface chemistry on its adsorption onto a flat interface of an oil-surfactant-water system. However, most studies have focused on equilibrium conditions when there is no flow in the system. 42,743 Under shear flow conditions, computations based on the lattice Boltzmann method have shown that nanoparticles or surfactants adsorbed at the droplet interface display exciting behavior.44 In this study, the drops were suspended in the middle of a channel and the motion of nanoparticles on the drop interface and their clustering under shear were investigated. The particles were spherical, neutrally wetting particles, which did not distribute homogeneously over the droplet surface and were found to not affect surface tension. The effects of shear on the migration of drops attached to a wall have not been investigated when both surfactants and nanoparticles are present and when the oil-water interface is modified. In this work, we seek to quantify the behavior of surfactants when they adsorb on an oil droplet and examine the displacement of this droplet immersed in water and under shear flow, with or without the presence of Janus particles. The dissipative particle dynamics (DPD) coarse-graining computational method is applied to simulate a shear flow under controlled conditions. The main research contributions are (a) to probe the effects of surfactants located at the oil-water interface on the migration of an oil droplet, (b) to examine the effects of JPs on the migration process, and (c) to understand the physical mechanisms of drop motion in the presence of both surfactants and Janus nanoparticles.

2. COMPUTATIONAL DETAILS

2.1. Dissipative Particle Dynamics. In a DPD model, point particles represent clusters of molecules rather than individual atoms.⁴⁵ The position and velocity of each DPD particle, which is often called a *bead*, can be calculated by Newton's equation of motion as follows

$$\frac{\mathrm{d}\mathbf{r}_{i}}{\mathrm{d}t} = \mathbf{v}_{i} \tag{1}$$

$$m_i \frac{\mathrm{d}\mathbf{v}_i}{\mathrm{d}t} = \mathbf{f}_i = \sum_{j \neq i} (\mathbf{F}_{ij}^{\mathrm{C}} + \mathbf{F}_{ij}^{\mathrm{D}} + \mathbf{F}_{ij}^{\mathrm{R}})$$
(2)

where \mathbf{r}_i , \mathbf{v}_i are the position and velocity vectors, respectively, m_i is the mass of bead i, and \mathbf{f}_i is the force vector acting on bead i. The total force exerted between two DPD particles i and j includes three components: the conservative (F_{ij}^{D}) , dissipative (F_{ij}^{D}) , and random (F_{ij}^{R}) forces⁴⁶ that can be calculated as follows

$$\mathbf{F}_{ij}^{C} = \begin{cases} a_{ij} \left(1 - \frac{r_{ij}}{r_c} \right) \hat{\mathbf{r}}_{ij} & \text{for } r_{ij} < r_c \\ 0 & \text{for } r_{ij} \ge r_c \end{cases}$$
(3)

$$\mathbf{F}_{ij}^{\mathrm{D}} = -\gamma w^{\mathrm{D}}(\mathbf{r}_{ij})(\hat{\mathbf{r}}_{ij} \cdot \mathbf{v}_{ij})\hat{\mathbf{r}}_{ij}$$
(4)

$$\mathbf{F}_{ij}^{\mathrm{R}} = \sigma w^{\mathrm{R}}(r_{ij})\theta_{ij}\hat{\mathbf{r}}_{ij} \tag{5}$$

Here, $\mathbf{r}_{ij} = |\mathbf{r}_i - \mathbf{r}_j|$, $\hat{\mathbf{r}}_{ij} = (\mathbf{r}_i - \mathbf{r}_j)/\mathbf{r}_{ij}$, $\mathbf{v}_{ij} = \mathbf{v}_i - \mathbf{v}_p$, and r_c is the cut-off radius indicating the distance over which a bead can affect its neighbors. The coefficient a_{ij} is called the repulsion coefficient and is related to the repulsion between the beads i and j. It controls the type of fluid interactions that are present in the simulated system, while parameter γ is related to friction (and the fluid viscosity) and σ is the amplitude of random motion of the beads. The weight functions w^D and w^R vanish for $r_{ij} > r_c$. They are related to each other and to the dissipation parameters, as shown by Español and Warren 48

$$w^{\mathrm{D}}(r) = [w^{\mathrm{R}}(r)]^{2}$$
 (6)

and

$$\sigma^2 = 2\gamma k_{\rm B}T\tag{7}$$

where T is the system temperature and $k_{\rm B}$ is the Boltzmann constant.

The dissipative weight function is determined as

$$w^{D}(r_{ij}) = \begin{cases} (1 - r_{ij})^{2}, & \text{for } r_{ij} < r_{c} \\ 0, & \text{for } r_{ij} \ge r_{c} \end{cases}$$
(8)

Finally, the term θ_{ij} is a Gaussian white noise function that is calculated as

$$\langle \theta_{ij}(t) \rangle = 0, \quad \langle \theta_{ij}(t)\theta_{kl}(t') \rangle = (\delta_{ik}\delta_{jl} + \delta_{il}\delta_{jk})\delta(t-t')$$
(9)

where t is the time, δ_{ij} is the Kronecker delta, and $\delta(t-t')$ is the Dirac delta function. ⁴⁸

2.2. Simulation Details. The software package Large-scale Atomic/Molecular Massively Parallel Simulator (LAMMPS) was used to perform all computations herein. A plane Couette flow was established in a channel with a height of $21r_c$ (in dimensionless DPD units). The driving force for the flow was applied by moving the top wall of the channel with a constant relative velocity v, while the bottom wall did not move. Using this process, a well-controlled shear flow field was generated. The no-slip boundary condition at the walls needed to be obeyed, while periodic boundary conditions were applied in the other two directions. Based on previous findings,²⁴ the noslip boundary condition was obtained by satisfying three conditions: (1) freezing the DPD beads of the walls relative to each other to create solid walls, (2) applying bounce-back boundary conditions not exactly at the walls but at a distance of 0.1 DPD unit away from the walls to prevent fluid beads from moving through the solid domain, and (3) increasing the friction coefficient for the solid-fluid interactions to be twice that of the fluid-fluid.

Each water bead (W) was generated by lumping together five water molecules. The oil phase was represented by heptadecane ($C_{17}H_{36}$) molecules. In the DPD formulation, each heptadecane molecule was constructed by three equal oil beads (O), as designated in Figure 1. For the computations

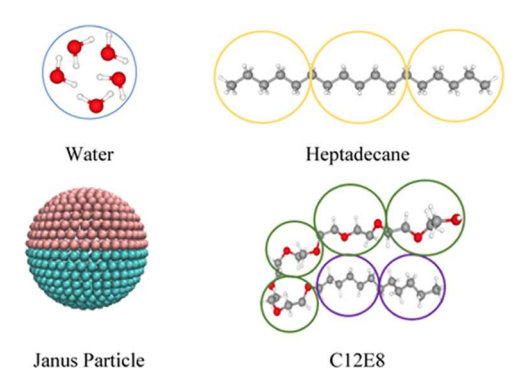


Figure 1. Schematic configuration of water, heptadecane, Janus particle, and C12E8 surfactant molecule as beads of the DPD simulations. Oxygen, hydrogen, and carbon are shown as red, white, and gray spheres, respectively. Cyan is the hydrophilic and pink is the hydrophobic surfaces of Janus particle beads.

with surfactants, the number of water molecules per bead increased to six, to ensure that the volume of the beads in all substances was comparable. The C12E8 surfactant molecule was represented by two hydrophobic tail (T) beads and four hydrophilic head (H) beads. Based on the C12E8 molecular structure, the tail-tail-head angle was fixed at 180° and all other angles between the beads were kept at 130° to meet the need for interfacial stability (see ref 22 for details). In the simulations, the JPs were considered spherical particles, consisting of two faces with distinct wetting properties. The JP beads were arranged with the distance between two neighboring beads set to $0.30r_c$ and the JP diameter was set at $4r_c$ (≈ 3.64 -nm-diameter particles because the length scale (r_c) of the computations was calculated to be 0.91×10^{-9} m). The conversion of time and length scales from DPD units to physical units is shown in Table 1. The NVE ensemble was used with temperature rescaling every 200 time steps and the Mach number for the computations was always less than 0.12. The schematic configuration of all species used in the DPD simulations is shown in Figure 1.

When the surfactant surface concentration is high, some surfactant molecules can partition out of the interface and create micelles in the water phase. Following the procedure detailed in our earlier work, the repulsion parameters used in the present study for the case of C12E8 at the oil—water interface, and the JPs at the oil—water interface, are listed in Table 2.

The Couette flow simulations were performed in a computational box with dimensions $50 \times 30 \times 21r_c^3$, in the x, y, and z directions (see Figure 2). The DPD water beads were placed between the two parallel solid plates in random locations. The computational domain shown in Figure 2 consisted of 4,788 wall beads and 156,000 fluid beads, and the density of the fluid in DPD units was 5 (i.e., the number of DPD beads per 1 unit volume of the simulation). The

Table 2. Details of the Various Repulsion Parameters (a_{ij}) Used in the Simulations^a

	Н	T	W	О	Pho	Phi	Wall
Н	15	25	14	25	54	15	35
T		15	54	14.5	15	54	15.5
W			15	100	54	15	25
O				15	15	54	20
Pho					15	54	15.5
Phi						15	35
Wall							15

"H and T represent the head and tail of the C12E8 surfactant, while W and O symbolize water and oil, respectively. The JPs include hydrophobic (Pho) and hydrophilic (Phi) beads.

surfactants and Janus particles were added to the surface of the oil droplet. The simulation time step was set to $\Delta t = 0.02$ in DPD units, and the total number of steps was 1,000,000 with an additional 10,000 time steps for the start-up period to reach equilibrium with no flow. Snapshots of the system were visualized by the visual molecular dynamics (VMD) software.⁵¹

2.3. Verification of Computations: Contact Angle and Size of Oil Droplets. The contact angle of a droplet is typically used to quantify the wetting of a solid by a liquid. Here, we present the contact angle for the oil droplet on the solid substrate; therefore, when the contact angle for the oil and the solid is smaller than the right angle $(\theta_{\text{oil}} < 90^{\circ})$, the surface is hydrophobic; if the droplet has a large contact angle $(\theta_{\text{oil}} > 90^{\circ})$, the oil droplet does not wet the solid wall and the surface is hydrophilic.

The surface tension between the fluids and the solid is related to the contact angle with Young's equation as follows

$$\gamma_{\rm SW} - \gamma_{\rm SO} = \gamma_{\rm OW} \cos \theta_{\rm oil} \tag{10}$$

where $\gamma_{\rm SW}$ is the solid wall—water surface tension, $\gamma_{\rm SO}$ is the solid wall—oil surface tension, $\gamma_{\rm OW}$ is the oil—water surface tension, and $\theta_{\rm oil}$ is the equilibrium three-phase contact angle of the oil drop on the solid substrate surrounded by water.

The fluid–fluid interfacial tensions, γ_{OW} , can be computed in the DPD computations based on the Kirkwood–Buff virial pressure method and the following formula⁵²

$$\gamma_{\text{OW}} = \frac{1}{2} L_z \left[P_{zz} - \frac{1}{2} (P_{xx} + P_{yy}) \right]$$
 (11)

Separate DPD simulations were conducted to calculate the surface tensions in eq 10. Layers of oil and water were distributed in a periodic box, thus two oil—water interfaces were employed to calculate the surface tension between oil and water, $\gamma_{\rm OW}$, using eq 11. The solid—fluid surface tensions were not calculated directly, instead their difference shown on the left-hand side of eq 10 was calculated. Two simulations were conducted for this purpose, one with the oil phase only and another with the water phase only between two solid walls, to obtain the quantity shown on the right-hand side of eq 11

Table 1. Scaling Factors for DPD Computations

additive on the interface	density	number of water molecules in one bead	mass scale (10 ⁻²⁵ kg)	$\begin{array}{c} \text{length scale} \\ \left(10^{-10} \text{ m}\right) \end{array}$	temperature scale (K)	time scale (10^{-12} s)
C12E8	5	6	1.80	9.66	298	6.38
C12E8 + JPs	5	6	1.80	9.66	298	6.38
JPs	5	5	1.50	9.09	298	5.48
none	5	5	1.50	9.09	298	5.48

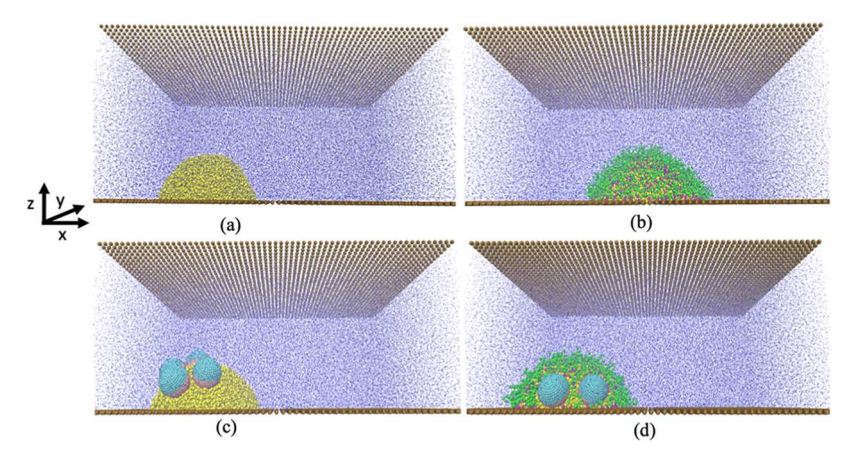


Figure 2. Snapshot of the oil droplet in the channel for various systems studied: (a) oil in water; (b) oil, water, and surfactant; (c) oil, water, and Janus nanoparticles; and (d) oil, Janus nanoparticles, surfactants, and water system. The wall, water, and oil beads are shown as ocher, blue, and yellow, respectively. Cyan color is representing the hydrophilic part of the JP, while pink is used for the hydrophobic face. Purple and green represent the tail and head beads of the surfactant, respectively.

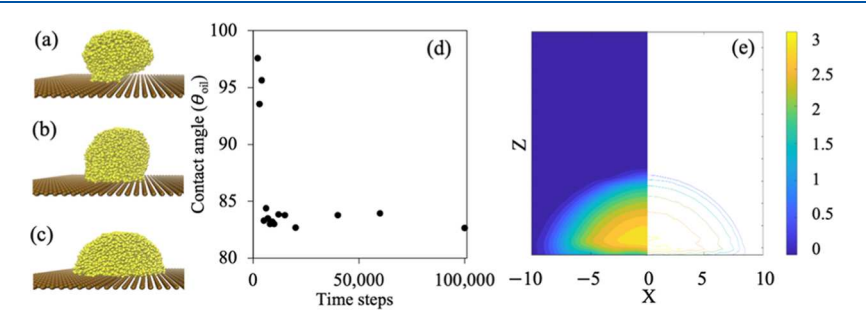


Figure 3. Equilibration of an oil drop (1944 oil molecules) on a solid wall at different stages of the DPD computation. (a) Drop after 500 time steps, (b) 1000 time steps, and (c) 10,000 time steps; (d) contact angle of the oil droplet in the water phase during the simulation time and (e) contour plot of oil droplet density at equilibrium.

for each of the cases of wall—oil and wall—water. The difference between these two, which is the quantity on the left-hand side of eq 10, was then calculated. Following the start-up period for each of these simulations, the interfacial tension values were determined every 100 time steps of the simulation and then averaged for 1,000,000 steps. These results were converted from the DPD units to real-world units using a scaling factor κ determined as $\kappa = \frac{\text{mass scale}}{\text{time scale}^2} = 4.98 \text{ mN/m}$. As a result, the interfacial tension value of heptadecane—water was computed as $\gamma_{\text{OW}} = 53.33 \text{ mN/m}$, which compares well with the experimentally reported value of $\gamma_{\text{OW}} = 53.20 \text{ mN/m}$, while $\gamma_{\text{SW}} - \gamma_{\text{SO}} = 8.42 \text{ mN/m}$. Using these values and eq 10, the contact angle for the oil droplet on the solid wall was calculated to be $\theta_{\text{oil}} = 80.9^{\circ}$.

To validate the computations, the contact angle of the oil droplet was also determined from the steady-state results of the DPD. The contact angle value for the oil drop reached equilibrium within 10,000 time steps in the computations (see Figure 3a–d). Finally, the contact angle of a drop on a flat surface was calculated directly from the density profile of the droplet and by using the sphere approximation and the ellipse approximation using the ImageJ software. As seen in Figure 3e, the value of the contact angle was found to be $\theta_{\rm oil} \approx 82.8^{\circ} \pm 1.1$, in good agreement with the value of the contact angle determined from Young's equation (i.e., 80.9°).

The contact angle when using a larger or smaller oil drop and a different simulation box size was also investigated, as shown in Figure 4. In Figure 4a, the contact angle was θ_{oil} =

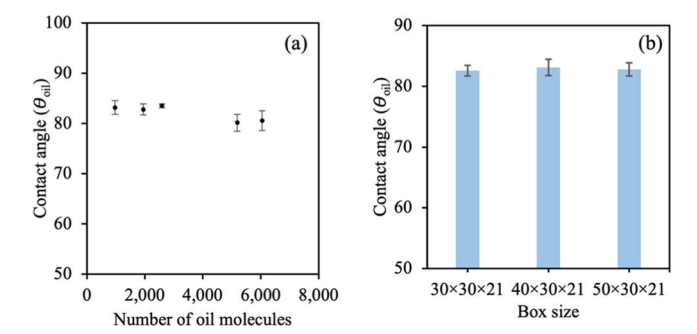


Figure 4. Dependence of the oil drop contact angle on the solid wall on the (a) number of oil molecules (box size: $x \times y \times z = 50 \times 30 \times 21$) and (b) size of the simulation box (1944 oil molecules).

 $82.0^{\circ} \pm 1.6$ for all cases studied with the number of oil molecules increasing from 972 to 6,048 molecules. As shown in Figure 4b, the size of the computational box does not affect the contact angle calculations, as expected when the properties of the fluids and the wall do not change. Therefore, we chose the biggest box for our simulations, while the number of oil molecules was set at 1,944 molecules (i.e., twice the number of oil molecules required to measure the contact angle). The contact angle for this case $(\theta_{\rm oil}=82.8^{\circ})$ had a smaller difference than that obtained from Young's equation.

3. RESULTS AND DISCUSSION

3.1. Effect of Surfactants Located at the Oil-Water **Interface.** Surfactants lower the IFT between oil and water, stabilizing the drop interface. To study the effect of their presence at the interface on drop migration, we added C12E8 molecules to the oil-water interface and subjected the drop to shear flow. The number of molecules added to the oil-water interface in these studies was determined as follows: The interfacial concentration of C12E8 on the heptadecane-water interface, corresponding to the critical micelle concentration (CMC), is 2.6×10^{-10} mol/cm^{2.55} In DPD units, this translates to 1.47 molecules per $1r_c^2$ of interfacial area for the system of C12E8 on an oil-water interface. Since we did not observe surfactant adsorption on the solid surface, the surface concentration of C12E8 at CMC was calculated as $N_{\rm CMC}$ = $1.47 \times S_{\rm O} = 1.47 \times 2\pi \frac{h^2}{1-\cos \theta_{\rm oil}} \approx 540$ molecules, where $S_{\rm O}$ is the area of the spherical cap that constitutes the oil-water interface. The drop interfacial area calculation was based on the measurement of the distance, h, from the solid wall to the highest point of the oil drop, and θ_{oil} used here is the equilibrium contact angle for the oil drop in the absence of surfactant molecules. The interfacial tension $\gamma_{\rm OW}$ and the threephase contact angle of the oil droplet in the presence of surfactants at interfacial concentrations up to the value corresponding to CMC are plotted in Figure 5a,b, respectively.

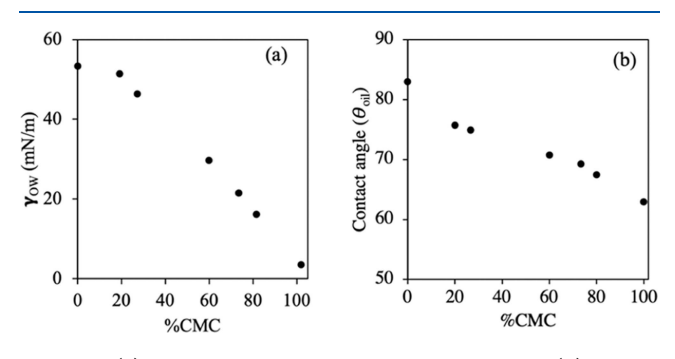


Figure 5. (a) Dependence of interfacial tension $\gamma_{\rm OW}$ and (b) contact angle ($\theta_{\rm oil}$) on the surface concentration of C12E8 normalized with its value at the CMC.

It was assumed that the number of C12E8 surfactant molecules per $1r_c^2$ for the case of heptadecane—water and hexadecane—water is approximately the same; 22 hence, the IFT at CMC for the case of C12E8 with hexadecane—water can be used for comparing with the case of heptadecane—water. The IFT for hexadecane—water at CMC of C12E8 was $\gamma_{\rm OW}\approx 3.33$ mN/m, 55 which was very close to our simulation result for heptadecane—water $\gamma_{\rm OW}\approx 3.55$ mN/m (see Figure 5a). In addition, it is seen that both $\gamma_{\rm OW}$ and $\theta_{\rm oil}$ decreased significantly with the concentration of the surfactant on the oil—water interface. Thus, the droplet spread more on the solid surface.

The drop migration results are provided in Figure 6 as a function of $\gamma_{\rm OW}$, where the concentration of the C12E8 surfactant was increased up to the CMC and the IFT was reduced accordingly (Figure 5a). The displacement of the drop was measured as the distance traveled by the drop center of mass (COM) during the simulation. The oil migration velocity, $V_{\rm O}$, was calculated based on the drop displacement and the time of the simulation (1,000,000 time steps after reaching equilibrium). Thus, it is the average migration

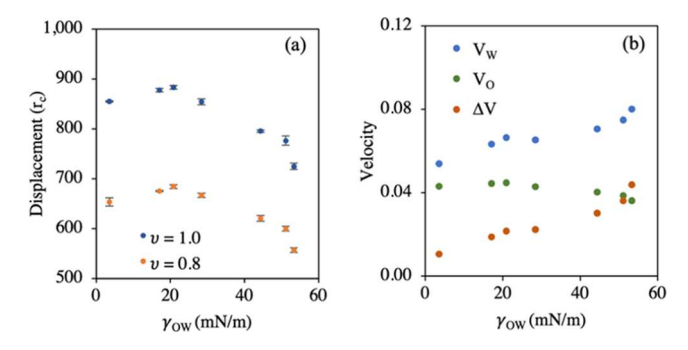


Figure 6. Effect of the oil—water interfacial tension ($\gamma_{\rm OW}$) on the oil drop migration. The $\gamma_{\rm OW}$ changes with addition of more surfactant to the interface; the highest $\gamma_{\rm OW}$ corresponds to the case of oil—water with no surfactant in the system, and the lowest $\gamma_{\rm OW}$ represents the case with surfactants at the CMC. (a) Displacement of the oil droplet for the duration of the simulation. Error bars indicate the standard deviation around the average value. (b) Slip velocity between the oil droplet and the water.

velocity of the drop for the time duration simulated. The velocity designated as $V_{\rm W}$ is the carrier fluid (water) velocity at a distance from the channel wall equal to the z location of the drop center of mass. The velocity profile for a plane Couette flow of a Newtonian fluid (water) is also known from theory to be changing linearly as a function of the distance from the stationary channel wall. So The velocity $V_{\rm W}$ was calculated from the DPD data at the z location that corresponds to the center of mass of the oil drop. Any difference between these two velocities $(V_{\rm O})$ and $V_{\rm W}$ indicates that the oil is lagging the surrounding water, and this difference is a measure of the slip between the two phases. As can be seen from Figure 6a, increasing the surfactant concentration (and decreasing the interfacial tension) led to an increase in the oil droplet displacement. For the case when the velocity of the top wall was 1.0, the displacement reached a maximum when the interfacial tension was $\gamma_{OW} \approx 20.84$ mN/m. This interfacial tension corresponded to surfactant concentration at the interface equal to 73.33% of CMC. Increasing the surfactant concentration further led to a slight decrease in the oil displacement until the concentration reached the CMC. The same trend was observed for the case of the top wall velocity v

These results can be explained by comparing the slip velocity between the oil droplet and the water, as shown in Figure 6b. When the γ_{OW} decreased from 53.33 mN/m (no surfactant) to 3.55 mN/m (at the CMC), the value of $V_{\rm W}$ went down because the drop shape changed. In order words, the center of mass of the droplet moved closer to the stationary channel wall in the z direction, as the drop spread out on the surface and the three-phase contact angle of the oil droplet reduced (see Figure 5b). The actual velocity of the droplet V_0 was found to increase up to a point and then it remained almost constant as the surfactant concentration reached CMC. The slip velocity ΔV decreased with a reduction in $\gamma_{\rm OW}$ values in the presence of higher surfactant concentrations. As the γ_{OW} decreased, the transfer of momentum between the two immiscible fluids became more efficient. Applying a linear fit between the γ_{OW} and the slip velocity ΔV between the oil droplet and water, it is found that $\Delta V = 0.0006\gamma_{\rm OW} + 0.0083$. Although the value of the coefficient of determination is not extremely high $(R^2 \approx$ 0.94), it is accepted to use a simple linear relationship since there is no physical justification for using a high-order

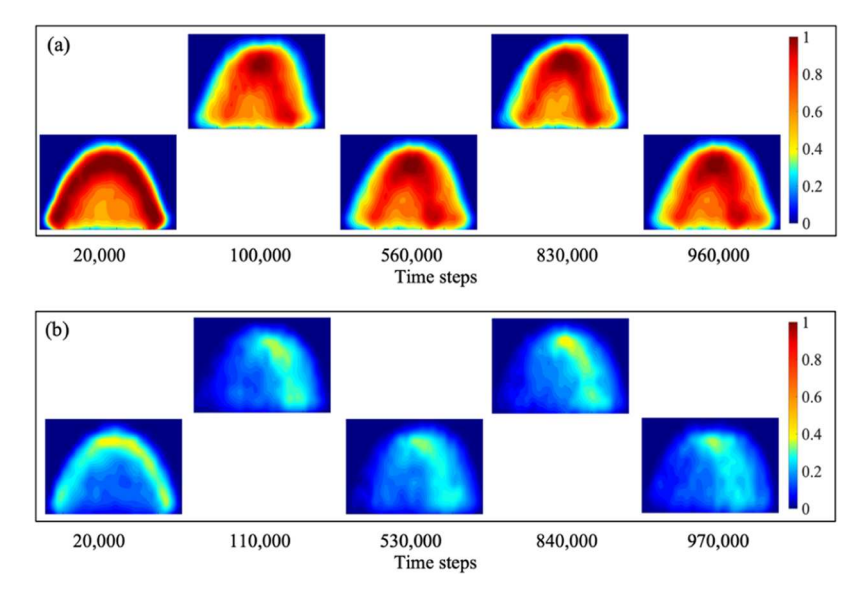


Figure 7. Color maps for the density of the surfactant at various times during the simulation for the case of surfactant concentrations at (a) CMC and (b) 26.67% CMC when the top wall moved with velocity v = 1.0. The start-up period is included in the time steps.

polynomial fit. The presence of a local maximum in the displacement as a function of γ_{OW} is also important to probe; therefore, we investigated the distribution of surfactant concentration on the droplet surface. Under the applied shear flow, the surfactant molecules moved from the front side (receding) to the rear side (advancing) on the drop surface, which results in low concentration on the front side and high concentration on the rear side. This migration generated a concentration gradient and a subsequent interfacial tension gradient on the oil drop-water interface, leading to Marangoni effects. The gradient in surfactant concentration can be observed clearly by examining snapshots of the surfactant distribution on the drop surface, as depicted in Figure 7. At high surfactant concentration ($C_{C12E8} > 75\%$ CMC), a reduction of the oil droplet displacement occurred (shown in Figure 6a) because the Marangoni stress created fluid motion at the interface. The driving force toward achieving a uniform surfactant distribution at the interface generated an interfacial velocity on the oil drop that was in the opposite direction to the shear flow (Figure 7a). Thus, the oil droplet tended to resist the flowing water, due to the interfacial flow from high to low surfactant concentration, causing a smaller displacement. In contrast, when the concentration of C12E8 is small, the surfactant concentration was more nonuniform on the surface of the oil drop (see Figure 7b); meanwhile, the influence of shear flow on the migration of the droplet was dominant. Hence, the effect of Marangoni flow was overwhelmed by the increase in momentum transfer and decrease in slip velocity. The main driving force of the oil movement was the impact of the water flow. This result agrees with previous reports. 57,58

3.2. Effects of Janus Particles and Surfactants on the Oil–Water Interface. To gain further insights into the physical mechanisms underlying the combined effects of the presence of Janus particles and surfactants on the drop motion in the microchannel, we conducted a detailed analysis of the JP particle motion on a drop surface with and without the surfactant. The number of C12E8 surfactant molecules was chosen to correspond to 73% of the CMC for the oil–water interface (i.e., 396 surfactant molecules added). There were two reasons for this choice. First, this concentration

corresponded to the maximum drop displacement, as described in the previous section, while mitigating the Marangoni effects. The second reason was to prevent surfactant molecules from desorbing from the oil—water interface to the aqueous phase and to avoid the creation of micelles. Such surfactant desorption could happen since the presence of JPs at the drop interface would decrease the interfacial contact area between oil and water. ⁴¹ Taking this into consideration, the effective surfactant concentration at the interface could exceed the surface concentration corresponding to the CMC if more than the 396 surfactant molecules were used.

In Figure 8, we show the position of JPs relative to the center of mass (COM) of the oil droplet. The difference

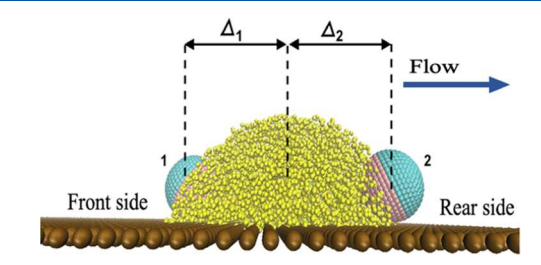


Figure 8. Position of Janus particles (JPs) compared to the center of mass (COM) of the oil droplet. Δ_1 is the distance between the COM of JP1 in the front side, while Δ_2 is the distance between the COM of the drop and the COM of JP2 on the rear side of the drop.

between the COM of a Janus particle i and the COM of the oil drop, Δ_{ij} was calculated as a function of simulation time as follows

$$\Delta_i = \text{COM}_{JP_i} - \text{COM}_{oil} \tag{13}$$

When the value of Δ_i is negative, the *i*-th JP is in front of the oil drop (as seen for JP1 in Figure 8), and when $\Delta_i > 0$, the JP was at the rear of the oil drop (see JP2 in Figure 8). Animations of the JP motion on the drop surface as a function of simulation time are provided in the Supporting Information

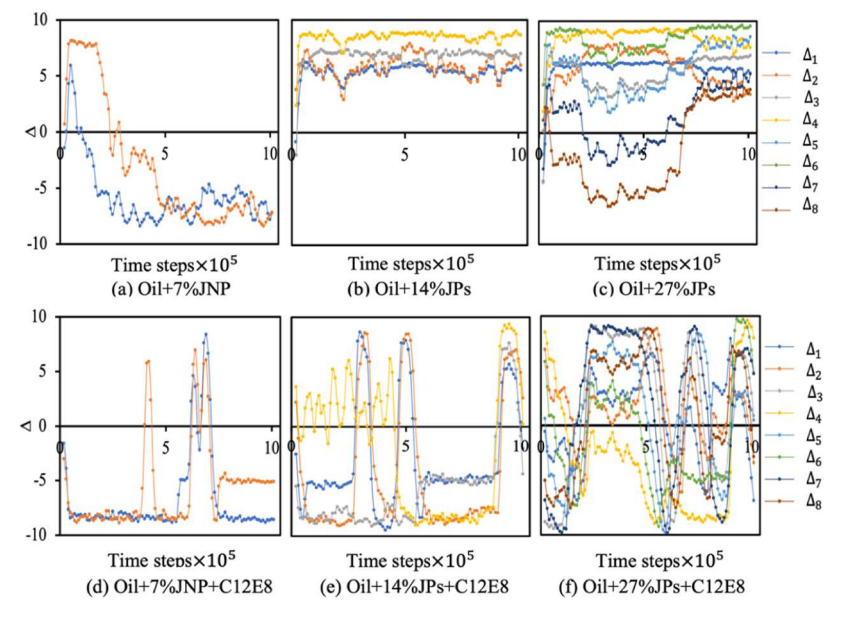


Figure 9. Trajectories of each JP relative to the center of mass of the droplet. Top row: No surfactant present and different JP coverages. Bottom row: 396 molecules of C12E8 present at the interface and different JP coverages.

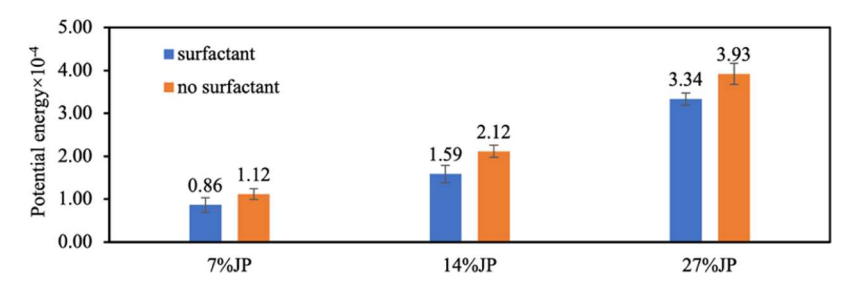


Figure 10. Total average potential energy of Janus particles and the solid bottom wall with C12E8 (blue) or without C12E8 (orange) at the interface between oil and water. The potential energy is in DPD units.

section. As the drop migrated, the JPs would move on the interface following specific patterns.

The relative position of each JP on the drop interface is plotted in Figure 9 as a function of time. Without the surfactant, the IPs would end up either at the front or at the rear of the drop and would remain close to each other because of the JP-JP interactions. The preferred location was close to the wall, at the oil-water-solid contact line, since JPs extending out of the drop experienced a hydrodynamic drag and moved away from the top of the drop and toward the drop sides. This behavior is seen in the top row of Figure 9, where all of the JPs are seen to settle at either negative or positive Δ . In marked contrast, when surfactants were also present at the interface, JPs tended to move from the front to the rear of the droplet and come back again in a periodic motion. This is seen in Figure 9d-f, where Δ changed sign periodically. We speculate that the reason for this periodic motion is the competition of hydrodynamic effects and Marangoni flow. The surfactant molecules move toward the front of the drop, but they also keep the JPs separated from each other. When JPs are at the front side of the drop, hydrodynamic resistance moves the JPs to the rear side of the drops (as was the case when the JPs were present without surfactants). When the JPs arrive at the rear side of the drop, the surfactants between the JPs cause them to stay separated from each other and to be at locations away from the hydrodynamic stagnation point at the rear side of the drop. The hydrodynamic forces and the Marangonidriven motion of surfactants then push the JPs to the front and the cycle is repeated. The ratio of the projection of a single JP in the direction of the flow over the projection of the oil drop on the direction of the flow is about 6% so that smaller JPs relative to the oil drop would experience smaller hydrodynamic forces. However, as the number of JP coverage increases, the periodic motion is manifested more clearly, indicating that the surfactants keep the JPs separated and away from the stagnation point at the rear side of the oil drop.

Because of how JPs moved with or without the presence of surfactants, they had different JP-bottom wall potential energy. The total potential energy of all IPs relative to the bottom wall was calculated and averaged over 1,000,000 time steps (shown in Figure 10). For every single case with the same number of IPs present, it is seen that the total IP-bottom wall potential energy in the case of only JPs is larger than the case when JPs co-existed with surfactants. Therefore, the motion of the droplet would become more difficult in the case of only Janus particles present at the oil-water interface. Furthermore, when particles assembled at the three-phase contact line of the drop with the bottom wall, the friction between them and the wall would impede the drop displacement. In comparison, surfactants can move freely, which helps to prevent the aggregation of JPs. As a result, the presence of surfactants aided the motion of Janus particles and resulted in a decrease in particle interaction with the wall.

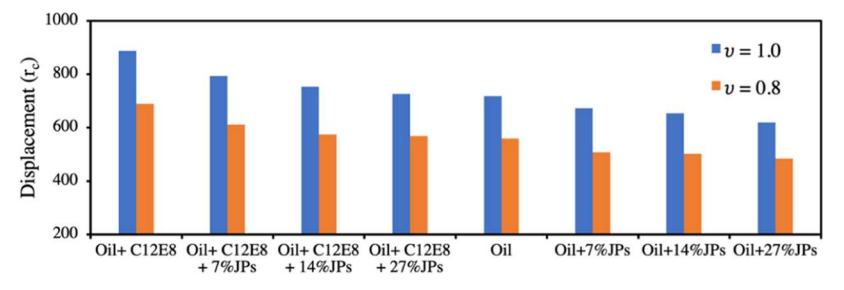


Figure 11. Displacement of the oil droplet in various cases.

Finally, the displacement of the oil droplet was calculated for all cases examined under Couette flow and is plotted in Figure 11. These included an oil droplet migrating in the water phase (designated as Oil in Figure 11), an oil droplet with the surfactant with concentration at 73% of the CMC (designated as Oil+C12E8), oil droplets with Janus particles at three different concentrations (designated as Oil + 7% JPs, Oil + 14% IPs, Oil + 27% IPs), and oil droplets-surfactants-Janus particles at 73% of the CMC and different JP concentrations (designated as Oil + C12E8 + 7%JPs, Oil + C12E8 + 14%JPs, Oil + C12E8 + 27%JPs). Each of these drops was subjected to the same shear flow conditions and for the same duration. It can be clearly seen that the drop migrated farther in the presence of both surfactants and Janus particles at the interface compared to the case of a bare oil droplet under shear. This was the case for both cases of top wall velocity in the Couette flow channel. Moreover, the more Janus particles were added to the oil droplet, the less the drop displacement. In addition, JPs experience lower water velocity around them when they assemble close to the oil-solid contact line, leading to a decrease in the speed of the particles.⁵⁹ Therefore, when more Janus particles were added, the displacement decreased.

4. CONCLUSIONS

In this study, we have numerically investigated the motion of an oil droplet with and without the presence of surfactants and Janus particles under shear flow conditions (Couette flow) by using the DPD simulation method. Under Couette flow, the presence of surfactants at the oil droplet surface leads to the largest migration velocity and displacement observed. The surfactants affect the interfacial tension, enhancing the momentum transfer from the water to the oil and reducing the oil—water slip. A linear relationship appears to apply between the slip velocity and the interfacial tension. Marangoni stresses tend to generate a motion of oil in the direction opposite to the direction of the shear flow, thus retarding the drop motion as a whole. However, with relatively small surfactant concentration, the effects of Marangoni stress are overwhelmed by the flow field.

It is demonstrated that Janus particles assemble at the drop-solid contact line, increasing the friction between the drop and the wall and increasing the potential energy for the interactions between the Janus particles and the wall. Hence, JPs slow down the drop migration. Finally, the displacement of the oil droplet in the presence of both Janus particles and surfactants at the interface was compared to the case of a bare oil droplet. Since Janus particles have less interaction with the solid wall in the presence of surfactants, and since the interfacial tension, in this case, is smaller than the bare oil case, the coexistence of surfactants and Janus particles leads to higher displacement than the case of bare oil.

ASSOCIATED CONTENT

Solution Supporting Information

The Supporting Information is available free of charge at https://pubs.acs.org/doi/10.1021/acs.jpcb.2c03670.

Animation of the case of a migrating oil drop with 8 JPs only, where the motion of the JPs toward the rear side of the drop is evident (MOV)

Animation of the case of a migrating oil drop with 8 JPs and surfactants on the oil—water interface, where the periodic motion of the JPs from the rear to the front of the drop is seen (MOV)

AUTHOR INFORMATION

Corresponding Authors

Sepideh Razavi — School of Chemical, Biological and Materials Engineering, The University of Oklahoma, Norman, Oklahoma 73019, United States; ocid.org/0000-0003-1225-6081; Email: srazavi@ou.edu

Dimitrios V. Papavassiliou — School of Chemical, Biological and Materials Engineering, The University of Oklahoma, Norman, Oklahoma 73019, United States; oorcid.org/0000-0002-4583-0820; Email: dvpapava@ou.edu

Author

Thao X. D. Nguyen – School of Chemical, Biological and Materials Engineering, The University of Oklahoma, Norman, Oklahoma 73019, United States

Complete contact information is available at: https://pubs.acs.org/10.1021/acs.jpcb.2c03670

Notes

The authors declare no competing financial interest.

ACKNOWLEDGMENTS

Acknowledgment is made to the donors of The American Chemical Society Petroleum Research Fund for partial support of this research through grant PRF # 58518-ND9 and the National Science Foundation (NSF-CBET) for grant CBET 1934513. The use of computing facilities at the University of Oklahoma Supercomputing Center for Education and Research (OSCER) and XSEDE (under allocation CTS-090025) is acknowledged.

REFERENCES

- (1) Seemann, R.; Brinkmann, M.; Pfohl, T.; Herminghaus, S. Droplet based microfluidics. *Rep. Prog. Phys.* **2011**, *75*, No. 016601.
- (2) Wegener, M.; Kraume, M.; Paschedag, A. R. Terminal and transient drop rise velocity of single toluene droplets in water. *AIChE J.* **2010**, *56*, 2–10.
- (3) Liu, K.; Jiang, L. Bio-inspired self-cleaning surfaces. *Annu. Rev. Mater. Res.* **2012**, 42, 231–263.

- (4) Yilbas, B. S.; Ali, H.; Al-Sharafi, A.; Al-Aqeeli, N.; Abu-Dheir, N.; Demir, K. Mobility of A Water Droplet on Liquid Phase of N-Octadecane Coated Hydrophobic Surface. *Sci. Rep.* **2018**, *8*, 1–13.
- (5) Angeli, P.; Hewitt, G. F. Drop size distributions in horizontal oilwater dispersed flows. *Chem. Eng. Sci.* **2000**, *55*, 3133–3143.
- (6) Datta, S.; Das, A.; Das, P. Uphill movement of sessile droplets by electrostatic actuation. *Langmuir* **2015**, *31*, 10190–10197.
- (7) Luo, X.; Yin, H.; Ren, J.; Yan, H.; Lü, Y.; He, L. Electrocoalescence criterion of conducting droplets suspended in a viscous fluid. *J. Phys. Chem. C* **2019**, *123*, 19588–19595.
- (8) Lazar, P.; Riegler, H. Reversible self-propelled droplet movement: A new driving mechanism. *Phys. Rev. Lett.* **2005**, 95, No. 136103
- (9) Sommers, A. D.; Brest, T.; Eid, K. Topography-based surface tension gradients to facilitate water droplet movement on laser-etched copper substrates. *Langmuir* **2013**, *29*, 12043–12050.
- (10) Guido, S.; Preziosi, V. Droplet deformation under confined Poiseuille flow. Adv. Colloid Interface Sci. 2010, 161, 89–101.
- (11) Fan, J.; Wilson, M.; Kapur, N. Displacement of liquid droplets on a surface by a shearing air flow. *J. Colloid Interface Sci.* **2011**, 356, 286–292.
- (12) Ding, H.; Spelt, P. D. Onset of motion of a three-dimensional droplet on a wall in shear flow at moderate Reynolds numbers. *J. Fluid Mech.* **2008**, *599*, 341–362.
- (13) Luo, Z. Y.; Shang, X. L.; Bai, B. F. Marangoni effect on the motion of a droplet covered with insoluble surfactant in a square microchannel. *Phys. Fluids* **2018**, *30*, No. 077101.
- (14) Liu, X.; Li, Y.; Tian, S.; Yan, H. Molecular dynamics simulation of emulsification/demulsification with a gas switchable surfactant. *J. Phys. Chem. C* **2019**, *123*, 25246–25254.
- (15) Lac, E.; Sherwood, J. Motion of a drop along the centreline of a capillary in a pressure-driven flow. *J. Fluid Mech.* **2009**, *640*, 27–54.
- (16) Nath, B.; Biswas, G.; Dalal, A.; Sahu, K. C. Migration of a droplet in a cylindrical tube in the creeping flow regime. *Phys. Rev. E* **2017**, 95, No. 033110.
- (17) Huang, C.-H.; Lee, E. Electrophoretic motion of a liquid droplet in a cylindrical pore. *J. Phys. Chem. C* **2012**, *116*, 15058–15067.
- (18) Horwitz, J.; Kumar, P.; Vanka, S. Three-dimensional deformation of a spherical droplet in a square duct flow at moderate reynolds numbers. *Int. J. Multiphase Flow* **2014**, *67*, 10–24.
- (19) Ahmadi, M. A.; Zendehboudi, S.; Shafiei, A.; James, L. Nonionic surfactant for enhanced oil recovery from carbonates: adsorption kinetics and equilibrium. *Ind. Eng. Chem. Res.* **2012**, *51*, 9894–9905.
- (20) Vu, T. V.; Papavassiliou, D. V. Modification of Oil—Water Interfaces by Surfactant-Stabilized Carbon Nanotubes. *J. Phys. Chem.* C 2018, 122, 27734—27744.
- (21) Shah, D. O. Improved Oil Recovery by Surfactant and Polymer Flooding; Elsevier, 2012.
- (22) Vu, T. V.; Papavassiliou, D. V. Oil-water interfaces with surfactants: A systematic approach to determine coarse-grained model parameters. *J. Chem. Phys.* **2018**, *148*, No. 204704.
- (23) Vu, T. V.; Razavi, S.; Papavassiliou, D. V. Effect of Janus particles and non-ionic surfactants on the collapse of the oil-water interface under compression. *J. Colloid Interface Sci.* **2022**, 609, 158–169.
- (24) Nguyen, T. X. D.; Vu, T. V.; Razavi, S.; Papavassiliou, D. V. Coarse Grained Modeling of Multiphase Flows with Surfactants. *Polymers* **2022**, *14*, 543.
- (25) Chevalier, Y.; Bolzinger, M.-A. Emulsions stabilized with solid nanoparticles: Pickering emulsions. *Colloids Surf., A* **2013**, 439, 23–34.
- (26) Dehghan Monfared, A.; Ghazanfari, M. H.; Jamialahmadi, M.; Helalizadeh, A. Potential application of silica nanoparticles for wettability alteration of oil—wet calcite: a mechanistic study. *Energy Fuels* **2016**, *30*, 3947–3961.

- (27) Al-Khafaji, A.; Neville, A.; Wilson, M.; Wen, D. Effect of low salinity on the oil desorption efficiency from calcite and silica surfaces. *Energy Fuels* **2017**, *31*, 11892–11901.
- (28) Yang, W.; Wang, T.; Fan, Z.; Miao, Q.; Deng, Z.; Zhu, Y. Foams stabilized by in situ-modified nanoparticles and anionic surfactants for enhanced oil recovery. *Energy Fuels* **2017**, *31*, 4721–4730
- (29) Tu, F.; Park, B. J.; Lee, D. Thermodynamically stable emulsions using Janus dumbbells as colloid surfactants. *Langmuir* **2013**, *29*, 12679–12687.
- (30) Lenis, J.; Razavi, S.; Cao, K. D.; Lin, B.; Lee, K. Y. C.; Tu, R. S.; Kretzschmar, I. Mechanical stability of polystyrene and janus particle monolayers at the air/water interface. *J. Am. Chem. Soc.* **2015**, *137*, 15370–15373.
- (31) Lan, Y.; Choi, J.; Li, H.; Jia, Y.; Huang, R.; Stebe, K. J.; Lee, D. Janus particles with varying configurations for emulsion stabilization. *Ind. Eng. Chem. Res.* **2019**, *58*, 20961–20968.
- (32) Razavi, S.; Lin, B.; Lee, K. Y. C.; Tu, R. S.; Kretzschmar, I. Impact of surface amphiphilicity on the interfacial behavior of Janus particle layers under compression. *Langmuir* **2019**, *35*, 15813–15824.
- (33) Correia, E. L.; Brown, N.; Razavi, S. Janus particles at fluid interfaces: Stability and interfacial rheology. *Nanomaterials* **2021**, *11*, 374
- (34) Qiao, Y.; Ma, X.; Liu, Z.; Manno, M. A.; Keim, N. C.; Cheng, X. Tuning the rheology and microstructure of particle-laden fluid interfaces with Janus particles. *J. Colloid Interface Sci.* **2022**, *618*, 241–247
- (35) Kozina, A.; Ramos, S.; Díaz-Leyva, P.; Castillo, R. Out-of-equilibrium assembly of colloidal particles at air/water interface tuned by their chemical modification. *J. Phys. Chem. C* **2016**, *120*, 16879–16886.
- (36) Carrasco-Fadanelli, V.; Castillo, R. Measurement of the capillary interaction force between Janus colloidal particles trapped at a flat air/water interface. *Soft Matter* **2020**, *16*, 5910–5914.
- (37) Eskandar, N. G.; Simovic, S.; Prestidge, C. A. Interactions of hydrophilic silica nanoparticles and classical surfactants at non-polar oil—water interface. *J. Colloid Interface Sci.* **2011**, 358, 217–225.
- (38) Wang, W.; Zhou, Z.; Nandakumar, K.; Xu, Z.; Masliyah, J. H. Effect of charged colloidal particles on adsorption of surfactants at oil—water interface. *J. Colloid Interface Sci.* **2004**, *274*, 625–630.
- (39) Nwidee, L. N.; Lebedev, M.; Barifcani, A.; Sarmadivaleh, M.; Iglauer, S. Wettability alteration of oil-wet limestone using surfactant-nanoparticle formulation. *J. Colloid Interface Sci.* **2017**, *504*, 334–345.
- (40) Nourafkan, E.; Hu, Z.; Wen, D. Nanoparticle-enabled delivery of surfactants in porous media. *J. Colloid Interface Sci.* **2018**, *519*, 44–57.
- (41) Vu, T. V.; Papavassiliou, D. V. Synergistic effects of surfactants and heterogeneous nanoparticles at oil-water interface: Insights from computations. *J. Colloid Interface Sci.* **2019**, *553*, 50–58.
- (42) Kirby, S. M.; Anna, S. L.; Walker, L. M. Effect of surfactant tail length and ionic strength on the interfacial properties of nanoparticle—surfactant complexes. *Soft Matter* **2018**, *14*, 112–123.
- (43) Katepalli, H.; John, V. T.; Bose, A. The response of carbon black stabilized oil-in-water emulsions to the addition of surfactant solutions. *Langmuir* **2013**, *29*, 6790–6797.
- (44) Frijters, S.; Günther, F.; Harting, J. Effects of nanoparticles and surfactant on droplets in shear flow. *Soft Matter* **2012**, *8*, 6542–6556.
- (45) Hoogerbrugge, P. J.; Koelman, J. Simulating microscopic hydrodynamic phenomena with dissipative particle dynamics. *Europhys. Lett. (EPL)* **1992**, *19*, 155.
- (46) Groot, R. D.; Warren, P. B. Dissipative particle dynamics: Bridging the gap between atomistic and mesoscopic simulation. *J. Chem. Phys.* **1997**, *107*, 4423–4435.
- (47) Pivkin, I. V.; Karniadakis, G. E. A new method to impose noslip boundary conditions in dissipative particle dynamics. *J. Comput. Phys.* **2005**, 207, 114–128.
- (48) Español, P.; Warren, P. Statistical mechanics of dissipative particle dynamics. *Europhys. Lett. (EPL)* **1995**, *30*, 191.

- (49) Plimpton, S. Fast parallel algorithms for short-range molecular dynamics. *J. Comput. Phys.* **1995**, *117*, 1–19.
- (50) Li, Y.; Guo, Y.; Bao, M.; Gao, X. Investigation of interfacial and structural properties of CTAB at the oil/water interface using dissipative particle dynamics simulations. *J. Colloid Interface Sci.* **2011**, 361, 573–580.
- (51) Humphrey, W.; Dalke, A.; Schulten, K. VMD: visual molecular dynamics. *J. Mol. Graphics* **1996**, *14*, 33–38.
- (52) Kirkwood, J. G.; Buff, F. P. The statistical mechanical theory of surface tension. *J. Chem. Phys.* **1949**, *17*, 338–343.
- (53) Rehfeld, S. J. Adsorption of sodium dodecyl sulfate at various hydrocarbon-water interfaces. J. Phys. Chem. A 1967, 71, 738–745.
- (54) Rasband, W. S. National Institutes of Health, Bethesda, Maryland, USA. http://imagej.nih.gov/ij/ 2011, Version 1.53a.
- (55) Rosen, M. J.; Murphy, D. S. Effect of the nonaqueous phase on interfacial properties of surfactants. 2. Individual and mixed nonionic surfactants in hydrocarbon/water systems. *Langmuir* **1991**, *7*, 2630–2635.
- (56) Bird, R. B. Transport phenomena. *Appl. Mech. Rev.* **2002**, *55*, R1–R4.
- (57) Bazhlekov, I. B.; Anderson, P. D.; Meijer, H. E. Numerical investigation of the effect of insoluble surfactants on drop deformation and breakup in simple shear flow. *J. Colloid Interface Sci.* **2006**, 298, 369–394.
- (58) Tang, X.; Xiao, S.; Lei, Q.; Yuan, L.; Peng, B.; He, L.; Luo, J.; Pei, Y. Molecular dynamics simulation of surfactant flooding driven oil-detachment in nano-silica channels. *J. Phys. Chem. B* **2019**, *123*, 277–288.
- (59) Sharan, P.; Postek, W.; Gemming, T.; Garstecki, P.; Simmchen, J. Study of Active Janus Particles in the Presence of an Engineered Oil—Water Interface. *Langmuir* **2021**, *37*, 204–210.

☐ Recommended by ACS

$\label{lem:controlled} Pressure-Controlled\ Layer-by-Layer\ to\ Continuous\ Oxidation\ of\ ZrS_2(001)\ Surface$

Liqiu Yang, Priya Vashishta, et al.

APRIL 13, 2023

ACS NANO

READ 🗹

Probing the Mechanism of Targeted Delivery of Molecular Surfactants Loaded into Nanoparticles after Their Assembly at Oil-Water Interfaces

Mohamed Amen Hammami, Emmanuel P. Giannelis, et al.

JANUARY 24, 2023

ACS APPLIED MATERIALS & INTERFACES

READ 🗹

Surface Phenomena with the Participation of Sulfite Lignin under Pressure Leaching of Sulfide Materials

Tatyana Lugovitskaya and Denis Rogozhnikov

APRIL 14, 2023

LANGMUIR

READ 🗹

Significantly Affected Lubrication Behavior of Silicone Oil Lubricated $\rm Si_3N_4/Glass$ Contact after Cleaning with Different Solvents

Xiangli Wen, Yu Tian, et al.

DECEMBER 23, 2022

LANGMUIR

READ 🗹

Get More Suggestions >